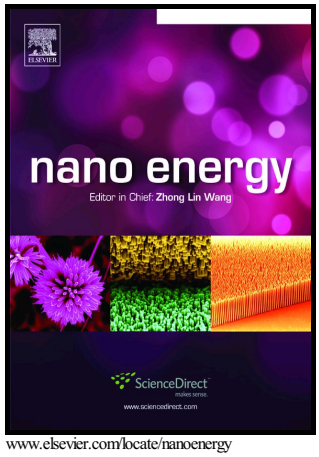

www.elsevier.com/locate/nanoenergy

Highly efficient perovskite solar cells for light harvesting under indoor illumination via solution processed SnO_2/MgO composite electron transport layers

Janardan Dagar, Sergio Castro-Hermosa, Giulia Lucarelli, Franco Cacialli, Thomas M. Brown

PII: S2211-2855(18)30257-X
DOI: https://doi.org/10.1016/j.nanoen.2018.04.027
Reference: NANOEN2657

To appear in: *Nano Energy*

Received date: 27 December 2017
Revised date: 11 March 2018
Accepted date: 9 April 2018

Cite this article as: Janardan Dagar, Sergio Castro-Hermosa, Giulia Lucarelli, Franco Cacialli and Thomas M. Brown, Highly efficient perovskite solar cells for light harvesting under indoor illumination via solution processed SnO_2/MgO composite electron transport layers, *Nano Energy,* https://doi.org/10.1016/j.nanoen.2018.04.027

Highly efficient perovskite solar cells for light harvesting under indoor illumination via solution processed SnO_2/MgO composite electron transport layers

Janardan Dagar,[a] Sergio Castro-Hermosa[a], Giulia Lucarelli[a], Franco Cacialli[b], Thomas M. Brown[a]' *

[a]CHOSE (Centre for Hybrid and Organic Solar Energy), Department of Electronic Engineering, University of Rome Tor Vergata, Via del Politecnico 1, 00133 Rome, Italy

[b]Department Physics and Astronomy and London Centre for Nanotechnology, University College London, London, WC1H 0AH, UK

Email: *thomas.brown@uniroma2.it

*thomas.brown@uniroma2.it

Corresponding Author

Abstract

We present new architectures in $CH_3NH_3PbI_3$ based planar perovskite solar cells incorporating solution processed SnO_2/MgO composite electron transport layers that show the highest power outputs ever reported under typical 200-400 lx indoor illumination conditions. When measured under white OSRAM LED lamp (200, 400 lx), the maximum power density values were 20.2 μW/cm^2 (estimated PCE = 25.0%) at 200 lx and 41.6 μW/cm^2 (PCE = 26.9%) at 400 lx which

correspond to a ~ 20% increment compared to solar cells with a SnO_2 layer only. The thin MgO overlayer leads to more uniform films, reduces interfacial carrier recombination, and leads to better stability. All layers of the cells, except for the two electrodes, are solution processed at low temperatures, thus low cost processing. Furthermore, ambient indoor conditions represent a milder environment compared to stringent outdoor conditions for a technology that is still looking for a commercial outlet also due to stability concerns. The unparalleled performance here demonstrated, paves the way for perovskite solar cells to contribute strongly to the powering of the indoor electronics of the future (e.g. smart autonomous indoor wireless sensor networks, internet of things etc).

KEYWORDS

electron transport layer, SnO_2 layer, SnO_2/MgO composite layer, planar perovskite solar cell, maximum power density, indoor light illumination.

Introduction

Organic lead halide perovskite solar cells (PSCs) have attracted great interest from the scientific and industrial communities due to rapid improvement in their photovoltaic performance as well as their low-cost and simple fabrication processes[1-6]. PSCs are prime candidates for harvesting light not only under natural sun light but also under artificial indoor light illumination, as recently demonstrated[7, 8], potentially providing power not only on large scale outdoor installations but also to operate small power electronic devices inside buildings [9-12] including autonomous sensors and wireless devices.[8, 13, 14] PSCs consist of multilayer structures where the perovskite layer is sandwiched between two transport layers, one for electrons (ETL) and one for holes (HTL). In order to obtain highly efficient and stable PSCs in the n-i-p configuration

different metal oxides including TiO_2, InO_3, ZnO and SnO_2 have been developed as ETLs over the bottom transparent electrode[4]. TiO_2 represents historically the initial and most common choice for ETL and can be modified with interlayers[15, 16]. However, more recently SnO_2 has come to the fore, having not only higher electron mobility but also high optical transparency and a wider energy band gap compared to TiO_2[17, 18]. The SnO_2 layer is deposited by spin coating and, importantly, annealed at low temperature which makes it useful also for developing PSCs on flexible substrates[19] or for modules with low embodied energy. Nevertheless, the performance of PSCs still suffers from surface trap states present at the interface of SnO_2 and the perovskite layer[20] which are responsible for charge recombination[21-23]. Solution-Processed SnO_2/MgO Composite Layer based perovskite solar cells have never been reported previously, with the exception of a very recent publication of which we became aware in the final stages of preparation of this manuscript[24] (nevertheless ours represents a new architecture for the ETL where the MgO is deposited over the SnO_2 leading to improved stability and unprecedented indoor performance as well as being deposited in more facile precursor liquid form in ethanol rather than nanoparticle form). Here we have introduced a thin layer of MgO (magnesium oxide) over the SnO_2 layer to tackle these issues and enhance further the performance of PSCs, reaching state of the art power conversion efficiency (PCE) under outdoor illumination and, we believe, the highest reported maximum power density for any photovoltaic cell under 200-400lx indoor illumination, both significantly higher than cells made with SnO_2 only ETLs. Furthermore, the shelf life stability was also improved using the composite ETL with the MgO overlayer.

Results and discussion

The device structure we developed is that of an ITO/SnO_2/MgO/$CH_3NH_3PbI_3$/Spiro-MeOTAD/Au planar PSCs (see figure 1(a)). The perovskite layer, $CH_3NH_3PbI_3$ was prepared via solvent engineering using a one-step spin coating process which lead to uniform and high quality films[25]. Spiro-MeOTAD (2,2',7,7'-tetrakis-(N,N-di-p-methoxyphenylamine)-9,9'-spirobifluorene) was used as HTL[22]. The SnO_2 ETL was deposited via spin coating over pre-cleaned ITO substrates according to optimized procedures [4, 26] to obtain a measured thickness of 24 nm. Crucially, we employed MgO as an interfacial layer[21] by spin coating a magnesium acetate tetrahydrate precursor solution in ethanol over the SnO_2 layer at different spin speeds (3k, 5k and 6k rpm, corresponding to thicknesses of ~30, 15 and 7 nm, respectively) to develop cells with the favourable thickness for the interlayer.

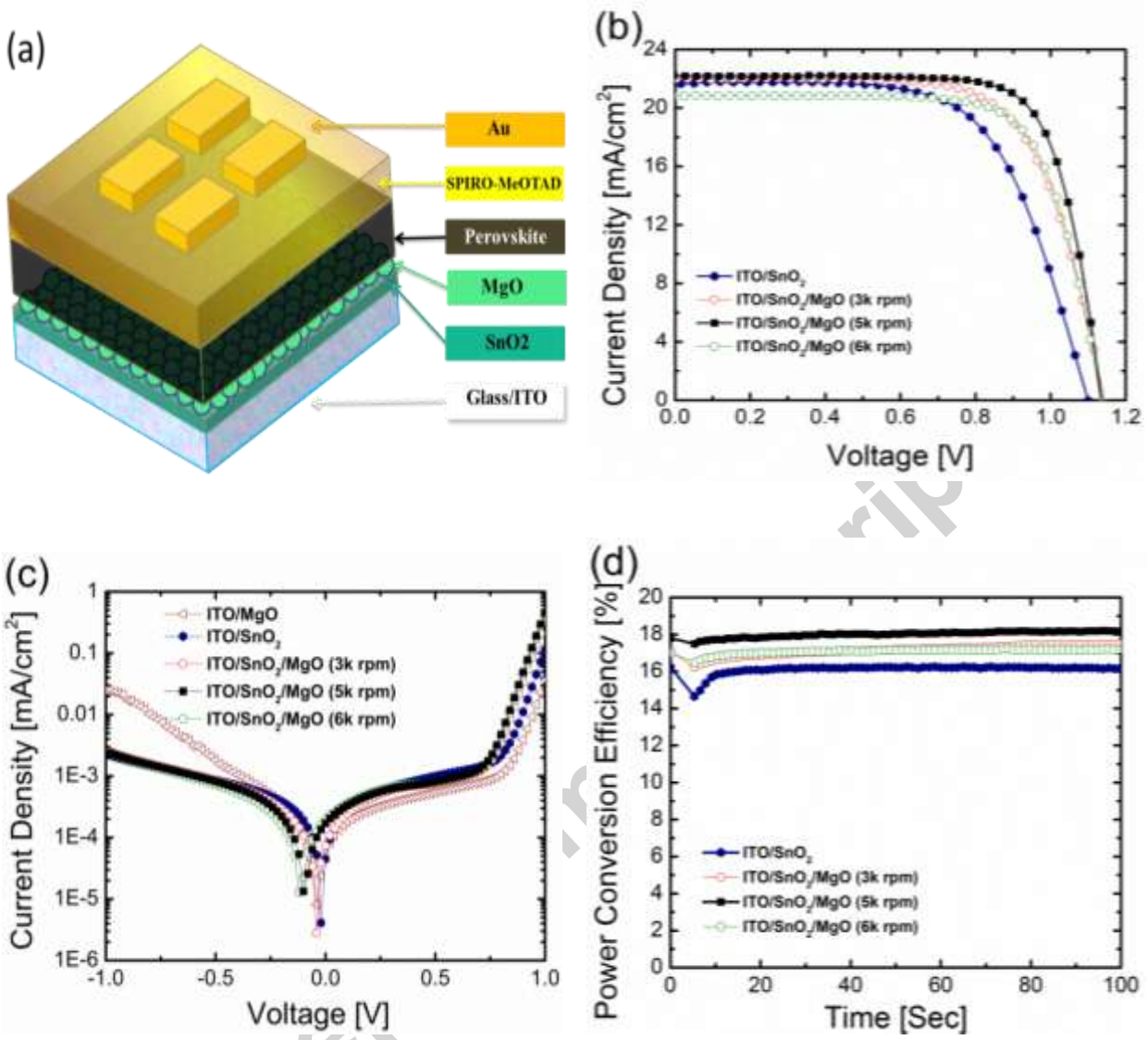

Figure 1. *(a) Schematic view of the ITO/SnO_2/MgO/$CH_3NH_3PbI_3$/Spiro-MeOTAD/Au planar perovskite solar cell device structure, (b) Best J-V curves of PSCs devices based on ITO/SnO_2 (navy blue solid hexagon) and ITO/SnO_2/MgO composite layers where the MgO interfacial layer was deposited by spin coating at different spin speeds, i.e. 3k rpm (red open circle), 5k rpm (black solid square), and 6k rpm (green open pentagon) under AM1.5G, 1000 W/m^2 irradiation, (c) J-V curves in the dark. (d) The evolution of the stabilized power conversion efficiency of the*

best PSCs over time measured at constant bias near the maximum power point under AM1.5G, 1000 W/m^2 irradiation.

The current density–voltage (*J-V*) characteristics at 1 sun of the best performing PSCs with the MgO interfacial layer deposited at different spin speeds are shown in figure 1 (b) together with those of cells made with just SnO_2 as ETL. The average values of PV parameters under 1 sun illumination, including short circuit current (J_{SC}), open circuit voltage (V_{OC}), fill factor (FF) and power conversion efficiency (PCE) are reported in Table 1 (a) and figure S1. The transmittance, reflectance and external quantum efficiency (EQE) spectra are reported in figure S3 (a), (b) and (c) together with the integrated photocurrent density of the EQE with the AM1.5G spectrum (Figure S3 (c)) which showed <10% discrepancy for both with and without MgO layer when compared with Jsc measured under 1sun. Tests were carried out on 12 different cells over 3 different batches for each type obtaining consistent results. The cells with only a MgO ETL show very poor performance (PCE = 0.75%). This is to be expected since the insulating MgO does not have a suitable electron affinity for electron extraction. The cells with a SnO_2-only ETL delivered an average PCE of 15.1% (and a maximum PCE of 15.3%) along with J_{SC} of 21.1 mA/cm^2, V_{OC} of 1.10V and FF of 64.8%. Incorporation of the MgO interfacial layers between the SnO_2 and the perovskite films led to considerable enhancements in PV performance: at the favourable spin speed (5k rpm), it was quantified to be 25% in relative terms with respect to the SnO_2 only counterparts resulting in an average PCE of 17.9% and a maximum PCE of 19.0%. Figure 1 (d) shows the steady-state efficiency of the same cells over time (100 seconds) measured at the fixed bias voltage of 0.785V for SnO_2 and 0.926V for SnO_2/MgO layer based PSCs corresponding to the maximum power point under 1 sun illumination. These steady state measurements show that the cells have good measurement stability. In the case of SnO_2/MgO,

the steady state value for the PCE was 18.1% which lies closer to the reverse sweep measurement (19.0%) compared to the forward one (16.1%) when measured under 1 sun.

It is interesting to note not only that the application of the SnO_2 and SnO_2/MgO layers over the ITO improve its transmittance (Figure S3 (a)) but also that the reflectance spectra (Figure S3 (b)) change when considering a full solar cell compared to just a glass/electrode sample where reflections occur not only at the bottom glass/air interface but also at the second glass/electrodes/air interfaces. These differences can be significant and can help explain apparent discrepancies when looking at transmittance of bare samples with EQE data from a full solar cell (Figure S3 (c)). For example, at 500 nm, the difference we measured in reflectance between the EQE of the full Glass/ITO/SnO_2/$CH_3NH_3PbI_3$/Spiro-MeOTAD/Au device (88.2%) and transmittance of the Glass/ITO/SnO_2 electrode (81.2%) is 7.0%. The difference in reflectance between the Glass/ITO/SnO_2 electrode and the full device is - 7.34% (i.e. the full device reflects less than the bare electrode so more photons are transmitted through to the active layers of the cell). At 550 nm the difference between EQE (90.22%) and Transmittance (85.67%) is -4.55 % and at 600 nm it is +1.0 % whereas the difference between the reflectance of the Glass/ITO/SnO_2 electrode and the full device are – 2.91 % and +1.94 % at 550nm and 600 nm respectively. Differences are within the measurement errors. Thus in the 430nm-570nm wavelength range, when a perovskite layer stack is added to the Glass/ITO/ETL substrate, reflection is decreased leading to a higher percentage of photons transmitted through the electrode (compared to the case of bare glass/electrodes) and into the active semiconductor augmenting its light harvesting capabilities. This is why EQEs can be higher and can reach peak threshold values of ~90%[27-30] on TCO-coated glass substrates. The refractive index of the new stack changes the reflectance pattern of the sample and can let in more photons compared to a bare glass/electrode

substrate[31]. This is indeed an interesting avenue of research which should be investigated more precisely and in depth in the future.

Table 1. *Averages of the PV parameters of $CH_3NH_3PbI_3$ planar perovskite solar cell devices based on ITO/MgO, ITO/SnO_2, ITO/SnO_2/SnO_2 and ITO/SnO_2/MgO composite layers with MgO interlayers deposited at different spin speeds. In brackets we report the values for the best cell.*

(a) under AM1.5G, 1000 W/m^2 irradiation.

Device	Light Source	Jsc [mA/cm^2]	Voc [V]	FF [%]	PCE [%]
ITO/MgO	AM 1.5 G	9.09 ± 0.98 (10.3)	0.289 ± 0.093 (0.337)	28.48 ± 1.60 (30.9)	0.746 ± 0.25 (1.08)
ITO/SnO_2	AM 1.5 G	21.10 ± 0.28 (21.3)	1.10 ± 0.003 (1.10)	64.82 ± 0.80 (64.9)	15.08 ± 0.41 (15.2)
ITO/SnO_2/SnO_2	AM 1.5 G	21.48 ± 1.36 (19.6)	1.07 ± 0.010 (1.08)	67.46 ± 7.51 (76.5)	15.48 ± 0.85 (16.3)
ITO/SnO_2/MgO (3k rpm)	AM 1.5 G	21.31 ± 0.61 (22.0)	1.13 ± 0.006 (1.14)	67.26 ± 2.29 (68.4)	16.26 ±0.88 (17.2)
ITO/SnO_2/MgO (5k rpm)	AM 1.5 G	21.26 ± 1.35 (22.1)	1.12 ± 0.018 (1.13)	74.78 ± 2.67 (75.7)	17.92 ± 1.32 (19.0)
ITO/SnO_2/MgO (6k rpm)	AM 1.5 G	20.59 ± 0.40 (20.8)	1.12 ± 0.004 (1.13)	72.27 ± 0.67 (72.8)	16.82 ± 0.44 (17.2)

(b) under 200 and 400 lx white LED light irradiation.

Device	Light Source	Jsc [µA/cm^2]	Voc [V]	FF [%]	PCE [%]	P_{Max} [µW/cm^2]
ITO/SnO_2	LED 200 lx	32.87 ± 0.99 (34.5)	0.836 ± 0.002 (0.840)	59.59 ± 0.70 (59.7)	20.23 ± 0.83 (21.40)	16.4 ± 0.67 (17.3)
ITO/SnO_2	LED 400 lx	62.99 ± 0.35 (63.3)	0.871 ± 0.004 (0.873)	58.30 ± 3.45 (61.4)	21.33 ± 0.57 (21.91)	32.0 ± 2.22 (34.0)

ITO/SnO_2/MgO (5k rpm)	LED 200 lx	32.84 ± 0.45 (33.3)	0.867 ± 0.006 (0.866)	69.69 ± 0.75 (70.0)	24.50 ± 0.31 (25.0)	19.8 ± 0.25 (20.2)
ITO/SnO_2/MgO (5k rpm)	LED 400 lx	63.21 ± 0.88 (64.5)	0.901 ± 0.004 (0.895)	72.04 ± 0.70 (72.0)	26.47 ±0.40 (26.9)	41.0 ± 0.62 (41.6)

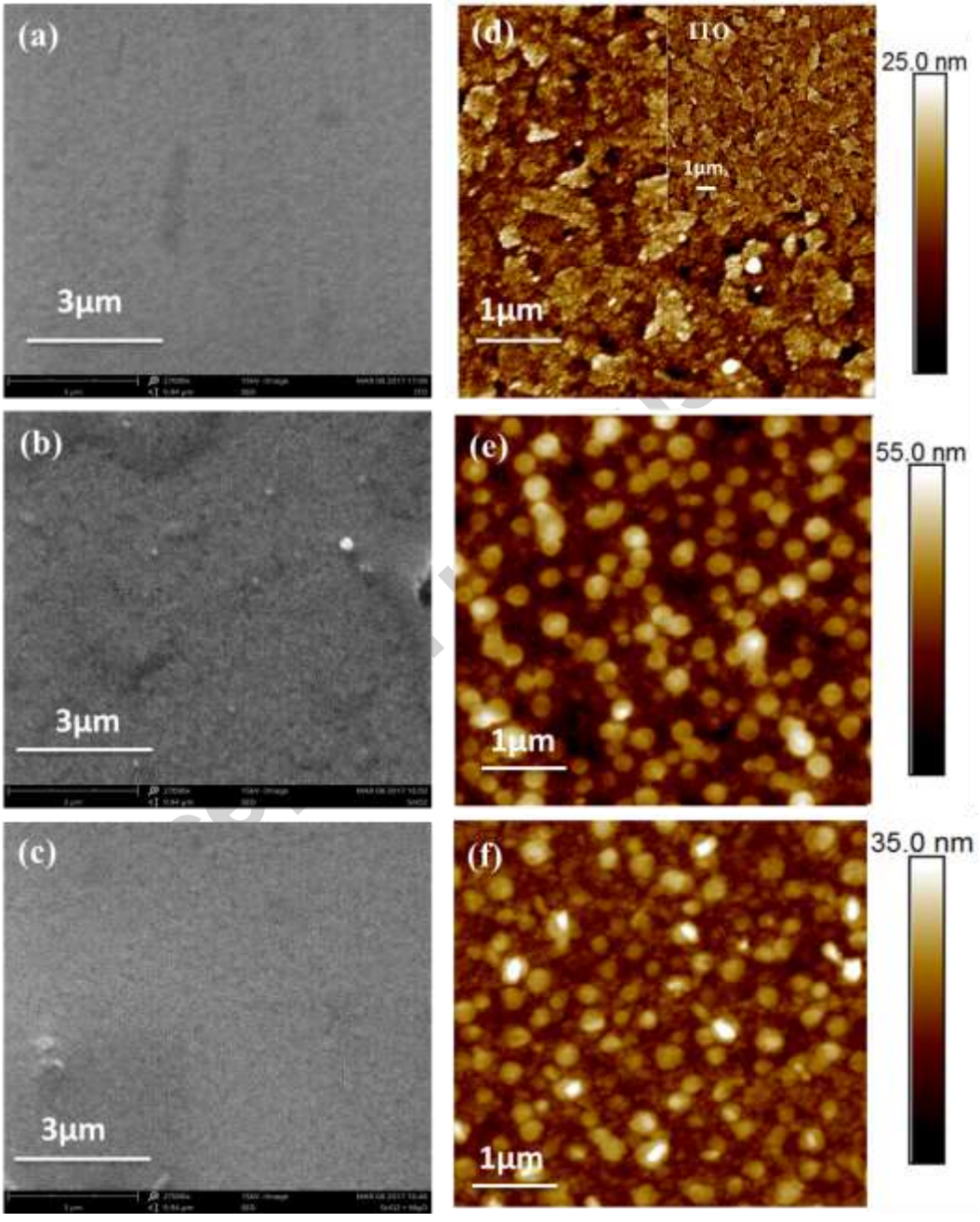

Figure 2. *Top view SEM images of (a) ITO only, (b) SnO_2 film deposited on ITO substrate (ITO/SnO_2) and (c) MgO layer deposited on ITO/SnO_2 surface (ITO/SnO_2/MgO). Atomic Force Microscopy (AFM) images of (d) ITO/MgO (together with ITO only, reported in inset), (e) ITO/SnO_2 and (f) ITO/SnO_2/MgO surface.*

EDX measurements of Figure S4 (a) and (b) clearly show the presence of MgO (Mg visible from the peak located at 1.25 Kev ionization energy is detected in the glass/ITO/SnO_2/MgO sample but not in the glass/ITO/SnO_2 sample) whereas the mapped elemental analysis (Figure S4 (c), (d) and (e)) suggests a relatively homogeneous coverage of the MgO over the SnO_2 since the intensity patterns of Mg are very similar to those of the underlying Sn which in turn are very similar to those of the underlying In (from the ITO). Scanning Electron Microscopy (SEM) and Atomic Force Microscopy (AFM) measurements were carried out to investigate the surface morphology and root mean square roughness of ITO-only, ITO/SnO_2 and ITO/SnO_2/MgO (see Figure 2). As shown in Figure 2 (a) and in the inset of Figure 2 (d), the bare ITO surface with roughness of 2.8 nm does not change even after MgO deposition (corresponding roughness was 2.9 nm), also suggesting that MgO produces a very thin conformal layer. The surface of the SnO_2 layer over ITO, appears corrugated with a relatively high surface roughness (~9.0 nm) and shows the presence of pinholes which act as surface defects (see Figure 2 (b) and (e)). The surface morphology appears more homogeneous after deposition of the MgO layer (5k rpm) as shown in Figure 2 (c) and (f). Interestingly, the surface roughness of the ITO/SnO_2/MgO layer was found to be ~5.1 nm, significantly lower than for ITO/SnO_2 (~9 nm). Thus, one of the roles played by the MgO layers is that of improving the film quality and of decreasing the probability of pinholes which can be responsible for the loss of charge carriers due to exciton recombination at defective interfaces[32]. Note that the application of the SnO_2 layer twice, which may be an alternative

route to decreasing the number of these recombination sites, does not lead to a similar enhancement in device performance (only by 7% in PCE), highlighting the crucial role of MgO as an interlayer. Thus the explanation of a higher V_{OC} delivered by solar cells upon application of the very thin MgO layer must contemplate its wide band gap electronic properties (a band gap of 8 eV) and its ability to enable tunneling of electrons from the perovskite to the ITO electrode whilst effectively blocking back-recombination and holes from migrating and recombining at the same electrode (thanks to a massively high barrier for holes as a result of an ionization potential of around 10 eV[33].

The most remarkable performance was observed when measuring the cells under indoor white LED light illumination. The *J-V* curves of the best PSC devices with SnO_2 and SnO_2/MgO (5k rpm) composite layers at 200 and 400 lx are displayed in figure 3 (a). The integration of the EQE with the white LED lamp spectrum has also been realized for indoor (Figure S7 (a) and (b)). The integrated Jsc show ≤17% discrepancy when compared to the Jsc obtained from white LED light spectrum at 200 and 400lx for SnO_2/MgO based PSCs, which is within the estimated error of our indoor measurement system[9]. The average PV parameters, including maximum power density (MPD), J_{SC}, V_{OC}, FF and PCE are summarized in table 1 (b) and table S1 (b) and figure S9. The PSCs with only SnO_2 as ETL provide an average value of MPD 16.4 μW/cm^2 (corresponding to an estimated PCE of 20.2 %) at 200 lx and of 32.0 μW/cm^2 (PCE = 21.3%) at 400 lx. These values were significantly enhanced with the incorporation of the MgO interlayer delivering an average MPD of 19.8 μW/cm^2 (PCE = 24.5 %) at 200 lx and 41.0 μW/cm^2 (PCE = 26.5%) at 400 lx. These values are at the very top for any photovoltaic technology reported as indoor light harvesters (see end of results and discussion section). Strikingly, whereas the cells with SnO_2

only ETL show large hysteresis under both 200 and 400 lx illumination, this is very strongly reduced for cells with the composite SnO_2/MgO ETL[16] (see figure 3(c)).

Because of potential hysteric behavior of PSCs, which depends on scan rates[34] (here kept consistent at 30 mV/s for all measurements) and history of the measurements, it is important to report the maximum power point tracking (MPPT) and the resulting steady state efficiency at constant bias voltage for our best performing cells based on a SnO_2/MgO ETL) also under indoor lighting; MPPT measurements were performed at 0.726 V at 200 lx and at 0.755 V at 400 lx; the results are displayed in figure 3 (d). The PSCs with SnO_2 only as ETL present a steady state PCE of 13.8% at 200 lx and 14.9% at 400 lx. These values are significantly lower that the PCE measured in reverse scan, due to the large hysteresis which can be seen in Figure 3 (b). In contrast, SnO_2/MgO based PSCs deliver a steady state PCE of 23.8% at 200 lx and 26.1% at 400 lx, which are much closer to the values extracted from the reverse scans due to a much lower hysteresis as visible in figure 3 (a) and Table S1.

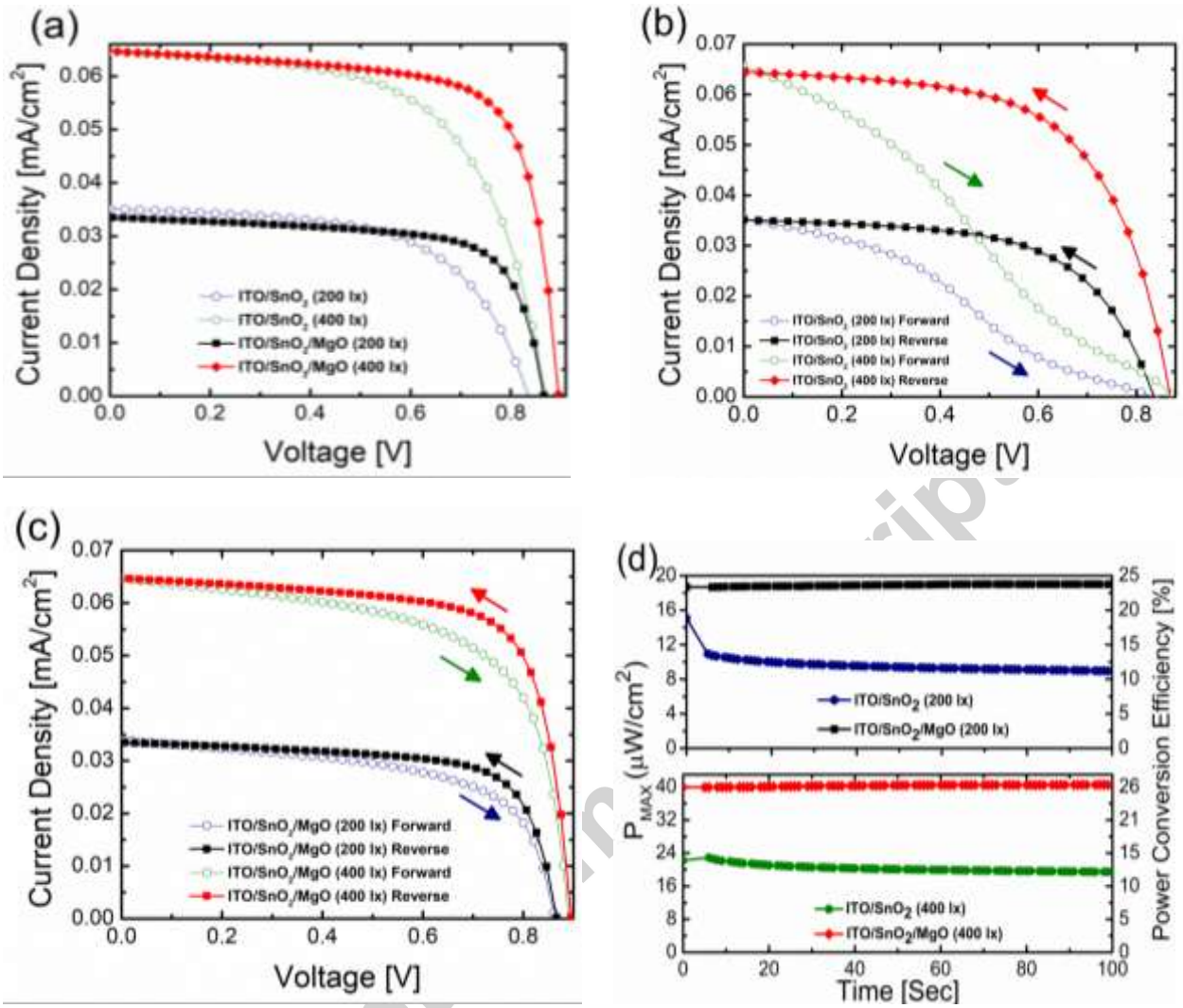

Figure 3. *(a) Current density-voltage curves of the best performing perovskite solar cell based on ITO/SnO_2 (both navy blue and green open circle), and ITO/SnO_2/MgO composite layers deposited at 5k rpm (both black and red solid square) under 200 and 400 lx white LED irradiation, (b) Best J-V curves of ITO/SnO_2 layer based PSCs under 200 and 400 lx in both forward and reverse bias scans, (c) Best J-V curves of ITO/SnO_2/MgO composite layer based PSCs under 200 and 400 lx in both forward and reverse bias scans. (d) The evolution of stabilized maximum power and corresponding power conversion efficiency of the best PSCs with*

either SnO_2 or SnO_2/MgO ETLs over time measured at constant bias at the initial maximum power point under 200 and 400 lx white LED irradiation.

The J-V dark curves provide useful information on the charge recombination and blocking process occurring at the interface between the electrode and perovskite layer of PSC devices[35] and are displayed in Figure 1 (c). PSCs using only MgO as ETL show poor rectification behavior. PSCs with SnO_2 ETLs show much higher rectification and comparatively low current density measured in reverse bias (i.e. at -1V applied voltage) resulting in good hole-blocking behavior because of adequate film forming properties and high energy barriers for holes[36]. The MgO-coated SnO_2 composite layer exhibited on/off current ratio (at +1V/-1V) of 3.02×10^2 which was significantly higher than that of the cell with only SnO_2 layer (8.27×10^1), leading to stronger rectification behavior. The optimum MgO layer over SnO_2 is very thin so that photo-generated electrons can be transported/tunnel through the MgO layer efficiently[23]. Looking at the whole batch of devices, higher rectification ratios are partly due to better blocking behavior (off currents of $(2.33 \pm 0.44)\times10^{-3}$ mA vs $(1.97 \pm 0.35)\times10^{-3}$ mA at -1 V for cells with SnO_2-only and SnO_2/MgO ETLs) but mainly to higher forward bias currents. The hole-blocking behavior of MgO which also leads to better V_{OC} as can be noted from Figure 1b is due to its very high ionization potential (~ 9-10 eV below vacuum)[32] which can improve the hole blocking behavior. The higher on currents in the dark together with the sizeable increase of FF (from 64.8% to 74.8%) under 1 sun is due to a balance of several factors[37] with the MgO interlayer on SnO_2 leading to a better contact resistance between the perovskite and the composite electrode due to a higher quality interface, possible doping of Mg resulting in surface segregation of MgO on SnO_2 which prevent the aggregation of SnO_2 and reduce the formation of pin holes [21, 38-40] as well as passivation of exciton recombination at such interface [33, 41]. The AFM

image of SnO_2 over ITO substrate (see figure 2 (e)) shows the imperfect surface morphology with high surface roughness (~9 nm), which can induce defective interface contact, thus leading to charge recombination at the SnO_2/perovskite interface. The insertion of the MgO layer (SnO_2/MgO/perovskite) may contributes to an improved interfacial contact by reducing the surface roughness to ~5.1 nm and therefore causing the retardation of recombination, thus leading to an enhancement of device performance [42, 43]. In fact the FF dependence on the ratio of charge extraction vs recombination has also been highlighted in other types of solar cells including organic and silicon solar cells. Adachi at el. reported that the retardation of charge recombination at interfaces leads to an increase of the fill factor [44, 45].

Open circuit voltage decay (OCVD) plots were used to better understand the recombination process occurring in PSC devices[46] and the results are reported in figure 4 (a). PSCs with a SnO_2/MgO composite layer take more time to be completely discharged (> 100 sec) compared to cells with a SnO_2 layer only, characterized by a shorter life time. Additionally, the OCVD measurements (Figure 4 (b)) under illumination show shorter rise times to arrive at the maximum V_{OC} (1.12V at 1.99 seconds) for the SnO_2/MgO composite layer compared to SnO_2 only cells (1.10V at 4.70 seconds). These results indicate that the MgO layer over SnO_2 passivates the surface traps and reduces fast charge recombination at the interface with the perovskite layer[47]. This leads to better photovoltaic performance under 1 sun and crucially, indoor conditions, where the quality of the ETL plays a major role, even greater than under 1 sun, in determining light harvesting performance [7, 8]. The J_{SC} vs incident light intensity (P_{in}) curves (see figure 4 (c)), also show a faster rise for the cells with the SnO_2/MgO ETLs, emphasizing a reduction in charge trapping paths[47] and improvement in electron injection at the interface of the perovskite and bottom electrode in PSCs[48]. Figure 4 (d) presents Voc vs P_{in} curves for both SnO_2 and

SnO_2/MgO based PSCs. The SnO_2/MgO based cell maintains a higher V_{OC} as a function of P_{in} in the whole measurement range, i.e. from 10^{-4} W/cm^2 (similar to indoor conditions) to 0.1W/cm^2 (i.e. 1 sun), compared to the SnO_2 based cell, especially under low levels of light illumination. The slope of Voc-P_{in} curve of SnO_2 based cell was 178 mV/dec in the low level 10^{-4}-10^{-3}W/cm^2 light intensity range whereas it was 98 mV/dec for the SnO_2/MgO based PSC showing a more rapid drop off. This behavior[7, 48] confirms that the MgO overlayer reduces recombination ensuring better performance of perovskite solar cells especially at low light intensities.

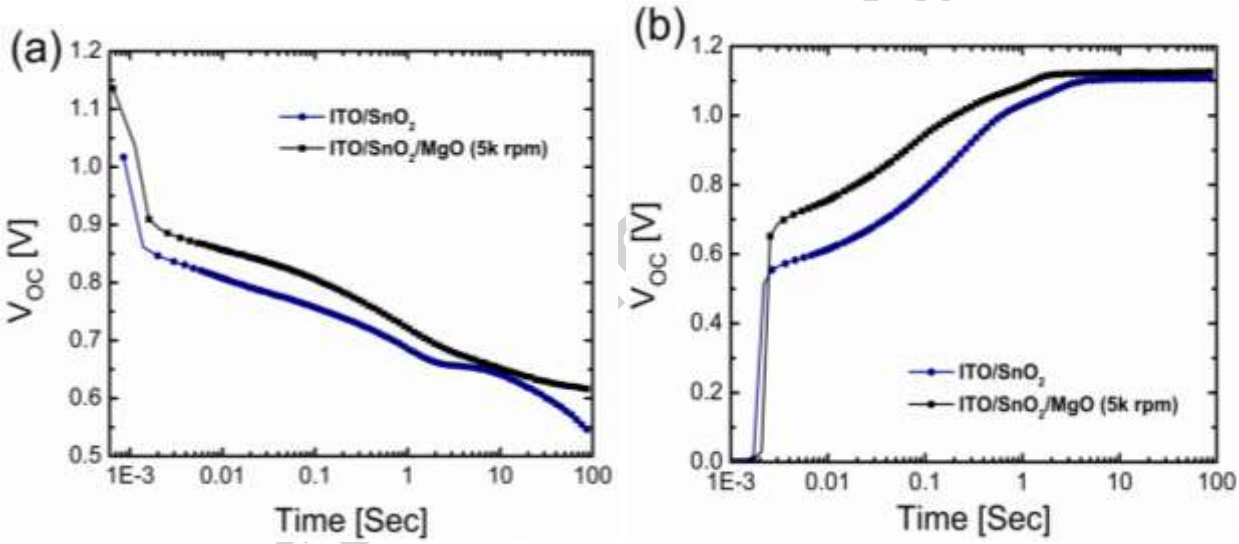

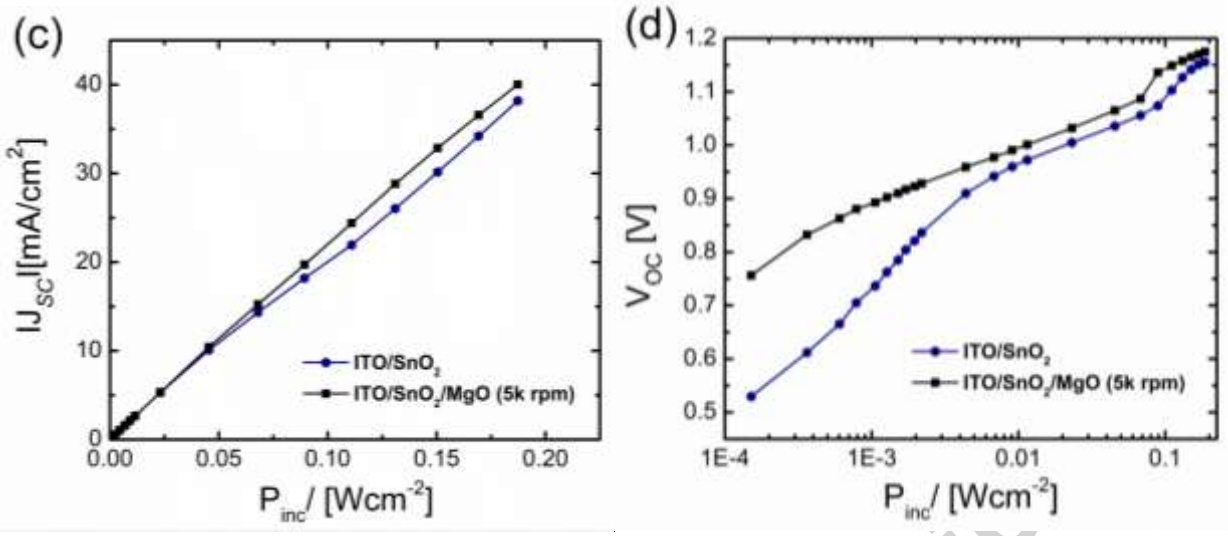

Figure 4. *Measurements of planar perovskite solar cell based on ITO/SnO_2 and ITO/SnO_2/MgO composite layers as ETLs. (a) Open Circuit Voltage Decay (OCVD) curves in dark, (b) OCVD curves under 1sun illumination, (c) Plot of current density verses* incident light intensity *($P_{inc/}$ [W.cm^{-2}]) and (d) plot of V_{OC} verses incident light intensity ($P_{inc/}$ [W.cm^{-2}]).*

We performed long-term shelf life stability tests on the sample with the four best PSCs incorporating either the SnO_2 or the SnO_2/MgO ETLs. The PSCs were stored in a dry box in air (relative humidity <30%) in the dark without any encapsulation to examine the shelf life stability over a period of 107 days. For each data point of Figure 5(a), the PCE for each of the four cells of each sample was measured under the solar simulator (ABET Sun 2000, class A) at standard test conditions (STC, i.e irradiance of 1,000 W/m^2, AM1.5G spectrum, and at 25 °C) using the reverse sweep in air. Notably, after 107 days, PSCs with the composite SnO_2/MgO layer maintain 68% of their initial average efficiency whereas those with only SnO_2 maintain 53% of their initial average PCE. The longer lifetimes can be ascribed to faster extraction of charges by the electrodes as well as more sturdy interlayers[49, 50]. We also carried out maximum power point tracking (MPPT) of the best performing SnO_2/MgO based cell (see figure 5 (b)) to monitor the steady state stability over the shelf life test. For this best cell, the stabilized maximum power

point on day 107 was 67.4% of that at day 0, confirming the results of the average PCE of Figure 5a. The J-V characteristics in the dark of Figure 5c show that the currents in reverse bias current (i.e. at -1V) for the cells with the SnO_2 only ETL have increased by 6 times compared to day 0 (see Figure 1c) whereas the cells with a SnO_2/MgO layer show comparatively less difference (i.e. only~2 times higher in relative terms) thus maintaining in time a better blocking behavior.

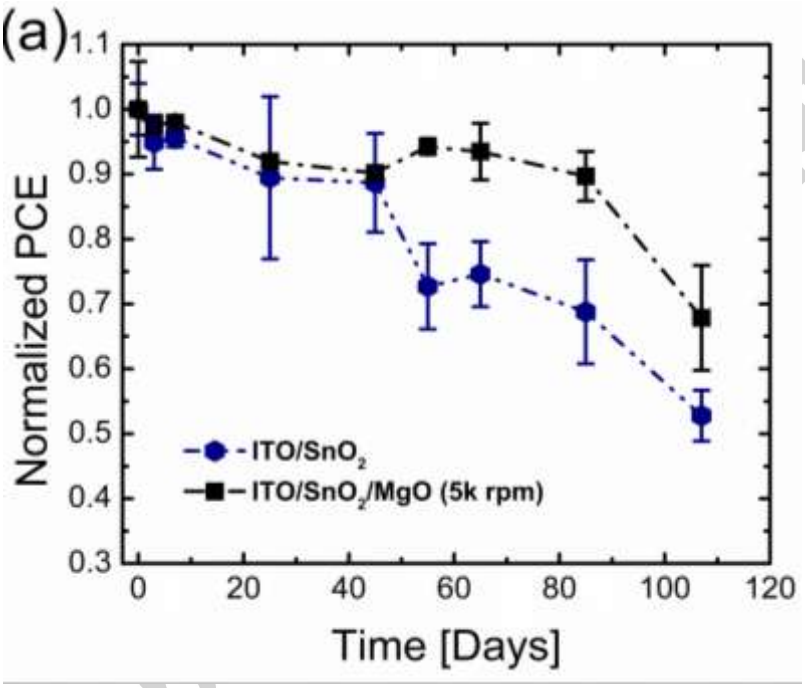

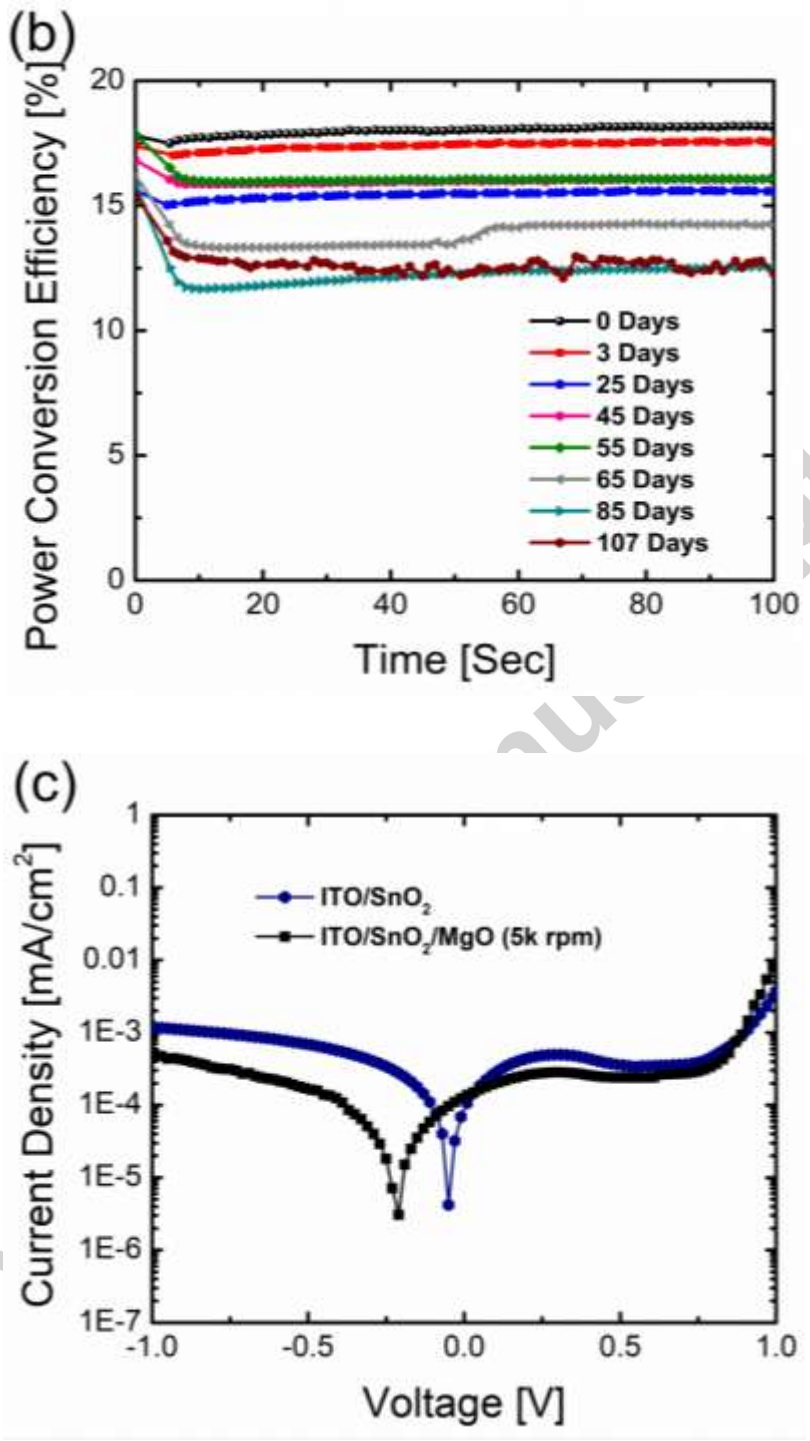

Figure 5. *(a) Shelf life stability Test of ITO/SnO_2/$CH_3NH_3PbI_3$/Spiro-MeOTAD/Au (blue solid circle) and ITO/SnO_2/MgO(5k rpm)/$CH_3NH_3PbI_3$/Spiro-MeOTAD/Au perovskite solar cell*

stored in a silica dry box without any encapsulation. (b) The evolution of best stabilized power conversion efficiency of ITO/SnO_2/MgO (5 krpm)/$CH_3NH_3PbI_3$/Spiro-MeOTAD/Au PSCs over time measured at constant bias near the maximum power point under AM1.5G, 1000 W/m^2 irradiation. (c) Dark J-V curves of ITO/SnO_2 and ITO/SnO_2/MgO(5k rpm) based PSCs after 107 days.

***Table 2**. Showing a comparison with other reports in the literature regarding the performance of perovskite solar cells under indoor illumination.*

Device	**Area (cm^2)**	**Light source**	**Illuminance (lux)**	**MPD (µA cm^{-2})**	**PCE (%)**
ALD-TIO_2-compact layer based mesoporous structured device [7]	0.12	CFL	200	15.4	24.0
			400	32.6	25.4
Inverted planar solar cell [51]	0.05	FL	100	-	22.5
			600	-	26.4
			1000	-	27.4
	5.44	FL	100	-	18.6
			1000	-	20.4
ALD-TIO_2 compact layer based mesoporous structured device (flexible) [8]	0.20	LED	200	10,8	7.2
			400	12,1	16.0
SnO_2 compact layer based	0.10	LED	200	12.9	9.8

mesoporous structured device (flexible) [20]			400	13.3	19.2
Planar SnO_2-based device, this work	0.10	LED	200	17.3	21.4
			400	34.0	17.3
Planar SnO_2/MgO-based device, this work	0.10	LED	200	20.2	25.0
			400	41.6	26.9

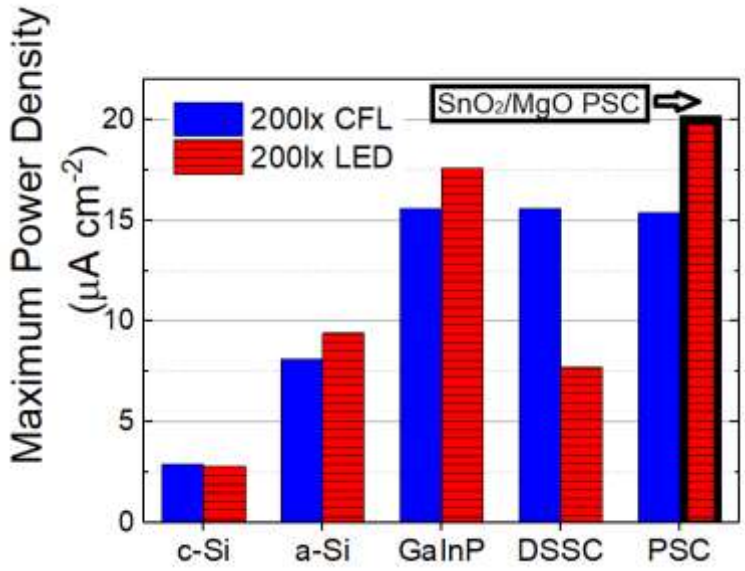

Figure 6. *Maximum power density of crystalline silicon (c-Si)[9, 10], amorphous silicon (a-Si)[3], GaInP[52], dye-sensitized solar cells (DSSC)[52, 53] and perovskite solar cells (PSC [7][5] reported in literature and the best planar SnO_2/MgO-based device developed in the present work (red bar furthest to the right); the values measured under 200 lx compact fluorescent light (CFL)*

illumination are displayed in plain blue, while the results obtained under 200 lx LED light are represented by red patterned bars.

To conclude our discussion, we highlight the outstanding performance of the perovskite solar cells incorporating the ITO/SnO_2/MgO electrodes as indoor light harvesters. Under indoor light conditions, the maximum power density (MPD) is a most important parameter which establishes which solar cell technology is valuable for applications such as consumer electronics, smart sensors etc requiring energy to be operated in indoor environments[9,52]. Efficiency values may suffer from higher estimated errors so it is important to provide both. Lux levels from artificial lighting typically range between 100-200lx in corridors/living rooms going up to 300-500 lx in office environments[9]. The values of MPD from our new architecture PSCs (average MPD was 19.8 μW/cm^2 at 200 lx corresponding to an estimated PCE of 24.5% and 41.0 μW/cm^2 at 400 lx with PCE of 26.5%) are significantly higher than previous reports for perovskite solar cells under indoor illumination in similar low light conditions (i.e. 200 lx and 400 lx) where the average MPDs were in the range of 14-15 μW/cm^2 (estimated PCE = 20-23%) and 30-32 μW/cm^2 (estimated PCE = 22-25%)[8, 19, 53]. A comparison with other reports in the literature regarding the performance of perovskite solar cells under indoor illumination is presented in Table 2 showing the unprecedented performance of the ITO/SnO_2/MgO-based perovskite solar cells in this work. At these lux levels the MPD of our devices also outperform the recent report[53] for the best dye sensitized solar cells which show an average MPD of 13.5μW/cm^2 (estimated PCE of 22.0%) at 200 lx. The efficiency is reported to increases when going to higher lux levels (e.g. 1000 lx) [51- 53] although one needs to consider the lower ranges when designing and sizing cells for general indoor use. As a final comparison at low light intensity (i.e. 200 lx), III-V semiconductor material the MPDs of GaInP and GaAs cells were 17.6μW/cm^2 and 16.6μW/cm^2

respectively [52]. The bar chart of Figure 6 presents the best MPDs for different photovoltaic technologies at 200 lx showing that the results of this work are at the very top for any photovoltaic technology. Furthermore, compared to our previous results[7, 8] which required chemical vapor deposition of high quality films compact blocking layers, not only performance is improved significantly but also achieved developing a completely solution processed ETL at low temperature which is conducive to low-cost high throughput and even web manufacturing.

Conclusion

We have shown new architectures of $CH_3NH_3PbI_3$ based planar perovskite solar cells incorporating SnO_2/MgO composite electron extracting layers between the ITO bottom electrode and perovskite semiconductor that achieve unprecedented power outputs under typical indoor illumination conditions. When measured under indoor white LED light illumination (200, 400 lx), the maximum power density values were 20.2 $\mu W/cm^2$ (estimated PCE = 25.0%) at 200 lx and 41.6 $\mu W/cm^2$ (PCE = 26.9%) at 400 lx which corresponded to ~ 20% increment compared to solar cells with a SnO_2 layer only. Such remarkable performance was achieved by inserting a thin MgO interfacial layer over the SnO_2 metal oxide layer which led to more uniform films as well as reducing interfacial carrier recombination. The maximum power conversion efficiency was 19.0% under 1 sun illumination of the best cell with a stabilized value of 18.1%. The MgO layer not only lead to higher rectification ratios but led to devices with considerably less hysteresis at low illuminance as well as better shelf life stability. Our approach is very simple (solution processed) and scalable and can be potentially transferred on flexible substrates. This paves the way for perovskite solar cells, which can provide highly efficient power outputs in these conditions as well as low cost (all layers are solution processed at low temperatures in our

cells except for the two conducting electrodes), to making small power devices autonomous, easily integrateable or even portable. The integration of cheap but efficient light harvesters can translate in a significant reduction of costs, both in terms of devices and maintenance, and also has a positive effect on the environment, reducing the impact associated to disposal of batteries[12]. At the moment, a huge number of electronic consumable products including RFID Tags, portable electronics, quartz oscillators, wireless sensor networks and wearable devices etc. are available in the market which need power (10nW-20μW)[52]. Perovskite solar cells may be able to provide the solution and thus contribute to the rapid expansion of applications such as autonomous indoor wireless sensor networks or embedded systems, and the Internet of Things.

Experimental Section

Materials:

Tin chloride ($SnCl_2.2H_2O$) dehydrate, Magnesium acetate tetrahydrate ($(CH_3COO)_2Mg.4H_2O$) and solvents DMSO (Dimethyl sulfoxide anhydrous, ≥99.9%), DMF (*N*,*N*-Dimethylformamide anhydrous, 99.8%), diethyl ether (99.0%), ethanol (99.8%) were purchased from Sigma-Aldrich. Lead(II) Iodide (99.99%, trace metals basis) was purchased from TCI Deutschland GmbH. Methylammonium iodide (CH_3NH_3I) was purchased from dyesol Ltd. 4-tert-butylpyridine (TBP), and Li-bis(trifluoromethanesulfonyl) imide (Li-TFSI) and cobalt(III) complex were purchased from Lumtec. 2,2',7,7'-tetrakis-(N,N-di-p-methoxyphenylamine)-9,9'-spirobifluorene (spiro-MeOTAD) (≥99.8%) was purchased from Borum New Material technology Ltd.

Device Fabrication:

At first, Glass/ITO substrates (Kintec -8Ω/□) were patterned with wet-etching in warm hydrobromic acid (HBr) solution masking the ITO with laser-cut black tape. Patterned Glass/ITO substrates were cleaned by ultrasonic bath, first in acetone and then in isopropanol solvents for 10 minutes at room temperature. For the fabrication of ITO/SnO_2/MgO/$CH_3NH_3PbI_3$/Spiro-MeOTAD/Au planar perovskite solar cell devices, SnO_2 solution was prepared by dissolving $SnCl_2 \cdot 2H_2O$ precursor in ethanol with resulting 0.1M concentration which was further stirred overnight at room temperature. SnO_2 electron transport compact layer was deposited on ITO coated glass substrate by two steps spin-coating process, first at the spin speed of 1500rpm for 30 seconds, leading further to 2500 rpm for next 30 seconds for obtaining 24nm thickness which was confirmed by profilometer. The SnO_2 film was finally annealed at 150 °C in air for 1 hour which was further kept in UV irradiation process with an estimated power density of 225 mW cm−2 (Dymax EC 5000 UV lamp with a metal-halide bulb PN38560 Dymax that contains no UV-C) for 15 minutes. The MgO solution was prepared by dissolving magnesium acetate tetrahydrate precursor in ethanol with 25mM concentration and stirred overnight at room temperature. The MgO interfacial layer was spin coated at different spin speeds including 3000, 5000 and the maximum 6000 rpm, for the optimization of the film thickness and annealed in air for 1 hour at 150 °C; films were then submitted to a UV light irradiation treatment for 15 minutes[21, 23]; the same procedure was followed for SnO_2 double layers.

The perovskite solution was prepared by dissolving 652.51mg PbI_2 and 225.05mg methylammonium iodide in the mixed solvents of 100.35µl DMSO and 899.65µl DMF (total 1ml) and stirred overnight at room temperature. The complete solution was spin coated on the ETLs first at 1000 rpm for 10 seconds with 5 acceleration, leading further to 5000 rpm for next 45 seconds with 5 acceleration; 0.7 ml of diethyl ether solvent was dropped on the rotating

substrate when 35 remained before surface became turbid, to obtain transparent perovskite films that were further annealed at 50 °C for 2 minute and 100 °C for next 10 minute to get dense black perovskite films[25]. Next, spiro-OMeTAD (73.5mg/mL) was dissolved in chlorobenzene solution and doped with TBP (26.77µL/mL), LiTFSI (16.6µL/mL), and cobalt(III) complex (7.2µL/mL) and kept overnight at room temperature. The spiro-OMeTAD solution was spin coated on the perovskite film at 2000 rpm for 20 seconds[48]. The samples were transferred in the metal evaporator where gold (Au) contacts were thermally evaporated through a shadow mask at a pressures below 10^{-6} mbar. Each substrate contained 4 devices of 0.1cm^2 area.

Characterization:

The UV–vis absorption spectra were recorded using UV–vis 2550 Spectrophotometer from Shimadzu.

EDX, and SEM microscopic images were captured from electron microscopy microscope (SEM Leo Supra 35) equipped with an INCAx-Sight Oxford Instruments X-EDS.

Reflectance spectrums were measured with a Shimadzu UV/VIS spectrophotometer (UV-2550) using and integrated sphere ISR-2200 which is placed inside of a multipurpose large sample compartment (MPC-2200). Integrated sphere allows the measurement of diffuse and specular reflection by combining angles of incident light of 0 and 8 degrees. The reflectance values of samples were calculated based on the barium sulphate (BaSO4) reference which presented a reflectance value equal to 100%. The incident light with an irradiation area of 2x3 mm^2 was focused at the centre of the samples under test which had a total area of 25x25 mm^2

Device Measurements:

Solar cell electrical characteristics were measured with a Keithley2420 source meter under an AM1.5G Class A ABET solar simulator at an intensity of 1000 W/m^2 (1 sun) calibrated with an ECO Pyranometer MS-602 at room temperature. The voltage step, scan speed and delay time for data point scans were fixed at 30 mV, 1 s, and 200 ms respectively for each cell measurements in both forward and reverse scan. Cells were masked with a black tape with 0.1cm^2 aperture during measurements. The EQE measurements were performed using IPCE (Incident Photon-to-current Conversion Efficiency) system (IPCE-LS200, Dyers) which has been calibrated using a UV-enhanced Si detector (Thorlabs, 250-1100nm)[54]. Stabilized power conversion efficiency over time was measured at constant bias at the maximum power point voltage under AM1.5G, 1000 W/m^2 irradiation using the LabVIEW software.. During the MPPT measurements of cells, we fixed the number of IV cycles (both forward and reverse) and scanning time (100 seconds).

For the indoor measurements of the perovskite devices, a customized setup with a white LED lamp (Osram Parathom Classic P25 4W daylight) was used as a light source with the illuminance levels (200 lx and 400 lx) adjusted by changing the distance of the samples from the LED light source as described in reference [7, 9]. In order to determine the different illuminance conditions prior to each measurement, we used a National Institute of Standard and Technology NIST-traceable calibrated Digisense 20250-00 light meter (due to its high level of accuracy). At each lux level, we also previously measured the irradiance spectrum with the International Light Technologies ILT900 NIST-traceable calibrated spectroradiometer from which the optical power density can be extracted to estimate the power conversion efficiency. In addition we also carried out integration of the EQE with the irradiance spectrum to verify that the Jsc was within the range of the experimental error of our measurement system [9]. Additionally, the geometric relation between the diameter of the light bulb, the distance from it to the platform, and the

active area of the solar cell means that in the worst case (illumination equal to 400 lx where the sample is closest to the light source), the deviation from the normal angle of incidence on the sample is only 3.2^{o}. The uniformity of illumination of our system is comparable with class B solar simulators [9]. Finally, we used a black scotch mask with aperture area equal to active area of solar cell during all measurements (area=0.1 cm^2).

Dark J-V characteristics, illumination intensity dependence of V_{OC} and Jsc and open circuit voltage rise/decay measurements were performed using a modular testing platform (Arkeo - Cicci research s.r.l.) which is composed of a white LED array (4200 K) tunable up to 200 mW/cm^2 of optical power intensity and high speed source meter unit. A spring contact based sample holder play an important role to improve the repeatability of the experiment. The voltage rise/decay measurements were performed in high perturbation configuration switching the light intensity from dark to 1 sun[7].

Supporting Information

Statistical PV parameters for planar perovskite solar cell device in sun light, Transmittance, Reflectance and External Quantum Efficiency measurements, EDX and SEM images, Schematic design of the indoor system, LED light spectrum, EQE for indoor, JV curve at constant bias near the maximum power point, summarized averages of the PV parameters under illumination of both sun and indoor light, statistical PV parameters for planar perovskite solar cell device in indoor light.

Acknowledgments

We thank Francesco Mura from University of Rome, La Sapienza for performing EDX and SEM measurements., Matteo Gasbarri, Francesco Di Giacomo, Fabio Matteocci, Lucio Cina, Emanuele Calabro, Dr Francesca Brunetti, Prof Andrea Reale and Prof Aldo Di Carlo for useful discussions. We thank MIUR for PRIN 2012 (2012A4Z2RY) ‘‘AQUASOL’’ (Celle solari polimeriche processabili da mezzi acquosi: dai materiali ai moduli fotovoltaici), the EU CHEETAH project and the Departamento del Huila's Scholarship Program No. 677 from Huila, Colombia for funding. FC is a Royal Society Wolfson Research Merit Award Holder.

Author Contributions

J.D. designed and fabricated the solar cell architectures, carried out their measurement, and contributed to writing the paper with S.C.H. S G. L. and F.C. carried out all the AFM measurements, analyzed the data and participated in writing the paper. T.M.B. envisioned and supervised the experiment and writing of the article.

References

[1] Green, M. A.;Ho-Baillie, A.; Snaith, H. J. The emergence of perovskite solar cells. *Nat Photon* **2014**, *8*, 506-514.

[2] Stranks, S. D.; Snaith, H. J. Metal-halide perovskites for photovoltaic and light-emitting devices. *Nat Nano* **2015**, *10*, 391-402.

[3] Dianetti, M.;Di Giacomo, F.;Polino, G.;Ciceroni, C.;Liscio, A.;D'Epifanio, A.;Licoccia, S.;Brown, T. M.;Di Carlo, A.; Brunetti, F. TCO-free flexible organo metal trihalide

perovskite planar-heterojunction solar cells. *Solar Energy Materials and Solar Cells* **2015**, *140*, 150-157.

[4] Ke, W.;Fang, G.;Liu, Q.;Xiong, L.;Qin, P.;Tao, H.;Wang, J.;Lei, H.;Li, B.;Wan, J.;Yang, G.; Yan, Y. Low-Temperature Solution-Processed Tin Oxide as an Alternative Electron Transporting Layer for Efficient Perovskite Solar Cells. *Journal of the American Chemical Society* **2015**, *137*, 6730-6733.

[5] Razza, S.;Castro-Hermosa, S.;Carlo, A. D.; Brown, T. M. Research Update: Large-area deposition, coating, printing, and processing techniques for the upscaling of perovskite solar cell technology. *APL Materials* **2016**, *4*, 091508.

[6] Tan, Z.-K.;Moghaddam, R. S.;Lai, M. L.;Docampo, P.;Higler, R.;Deschler, F.;Price, M.;Sadhanala, A.;Pazos, L. M.;Credgington, D.;Hanusch, F.;Bein, T.;Snaith, H. J.; Friend, R. H. Bright light-emitting diodes based on organometal halide perovskite. *Nat Nano* **2014**, *9*, 687-692.

[7] Di Giacomo, F.;Zardetto, V.;Lucarelli, G.;Cinà, L.;Di Carlo, A.;Creatore, M.; Brown, T. M. Mesoporous perovskite solar cells and the role of nanoscale compact layers for remarkable all-round high efficiency under both indoor and outdoor illumination. *Nano Energy* **2016**, *30*, 460-469.

[8] Lucarelli, G.;Di Giacomo, F.;Zardetto, V.;Creatore, M.; Brown, T. M. Efficient light harvesting from flexible perovskite solar cells under indoor white light-emitting diode illumination. *Nano Research* **2017**, 10.1007/s12274-016-1402-5, 1-16.

[9] De Rossi, F.;Pontecorvo, T.; Brown, T. M. Characterization of photovoltaic devices for indoor light harvesting and customization of flexible dye solar cells to deliver superior efficiency under artificial lighting. *Applied Energy* **2015**, *156*, 413-422.

[10] Li, Y.;Grabham, N. J.;Beeby, S. P.; Tudor, M. J. The effect of the type of illumination on the energy harvesting performance of solar cells. *Solar Energy* **2015**, *111*, 21-29.

[11] Reich, N. H.;van Sark, W. G. J. H. M.;Alsema, E. A.;Lof, R. W.;Schropp, R. E. I.;Sinke, W. C.; Turkenburg, W. C. Crystalline silicon cell performance at low light intensities. *Solar Energy Materials and Solar Cells* **2009**, *93*, 1471-1481.

[12] Freunek, M.;Freunek, M.; Reindl, L. M. Maximum efficiencies of indoor photovoltaic devices. *IEEE Journal of Photovoltaics* **2013**, *3*, 59-64.

[13] Matiko, J. W.;Grabham, N. J.;Beeby, S. P.; Tudor, M. J. Review of the application of energy harvesting in buildings. *Measurement Science and Technology* **2014**, *25*, 012002.

[14] Zhan, Y.;Mei, Y.; Zheng, L. Materials capability and device performance in flexible electronics for the Internet of Things. *Journal of Materials Chemistry C* **2014**, *2*, 1220-1232.

[15] Wojciechowski, K.;Stranks, S. D.;Abate, A.;Sadoughi, G.;Sadhanala, A.;Kopidakis, N.;Rumbles, G.;Li, C.-Z.;Friend, R. H.;Jen, A. K. Y.; Snaith, H. J. Heterojunction Modification for Highly Efficient Organic–Inorganic Perovskite Solar Cells. *ACS Nano* **2014**, *8*, 12701-12709.

[16] Chen, B.;Yang, M.;Priya, S.; Zhu, K. Origin of J–V Hysteresis in Perovskite Solar Cells. *The Journal of Physical Chemistry Letters* **2016**, *7*, 905-917.

[17] Tiwana, P.;Docampo, P.;Johnston, M. B.;Snaith, H. J.; Herz, L. M. Electron Mobility and Injection Dynamics in Mesoporous ZnO, SnO2, and TiO2 Films Used in Dye-Sensitized Solar Cells. *ACS Nano* **2011**, *5*, 5158-5166.

[18] Snaith, H. J.; Ducati, C. SnO2-Based Dye-Sensitized Hybrid Solar Cells Exhibiting Near Unity Absorbed Photon-to-Electron Conversion Efficiency. *Nano Letters* **2010**, *10*, 1259-1265.

[19] Di Giacomo, F.;Fakharuddin, A.;Jose, R.; Brown, T. M. Progress, challenges and perspectives in flexible perovskite solar cells. *Energy & Environmental Science* **2016**, *9*, 3007-3035.

[20] Dagar, J.;Castro-Hermosa, S.;Gasbarri, M.;Palma, A. L.;Cina, L.;Matteocci, F.;Calabrò, E.;Di Carlo, A.; Brown, T. M. Efficient fully laser-patterned flexible perovskite modules and solar cells based on low-temperature solution-processed SnO2/mesoporous-TiO2 electron transport layers. *Nano Research* **2017**, 10.1007/s12274-017-1896-5.

[21] Kulkarni, A.;Jena, A. K.;Chen, H.-W.;Sanehira, Y.;Ikegami, M.; Miyasaka, T. Revealing and reducing the possible recombination loss within TiO2 compact layer by incorporating MgO layer in perovskite solar cells. *Solar Energy* **2016**, *136*, 379-384.

[22] Tan, H.;Jain, A.;Voznyy, O.;Lan, X.;García de Arquer, F. P.;Fan, J. Z.;Quintero-Bermudez, R.;Yuan, M.;Zhang, B.;Zhao, Y.;Fan, F.;Li, P.;Quan, L. N.;Zhao, Y.;Lu, Z.-H.;Yang, Z.;Hoogland, S.; Sargent, E. H. Efficient and stable solution-processed planar perovskite solar cells via contact passivation. *Science* **2017**, 10.1126/science.aai9081.

[23] Guo, X.;Dong, H.;Li, W.;Li, N.; Wang, L. Multifunctional MgO Layer in Perovskite Solar Cells. *ChemPhysChem* **2015**, *16*, 1727-1732.

[24] Ma, J.;Yang, G.;Qin, M.;Zheng, X.;Lei, H.;Chen, C.;Chen, Z.;Guo, Y.;Han, H.;Zhao, X.; Fang, G. MgO Nanoparticle Modified Anode for Highly Efficient SnO2-Based Planar Perovskite Solar Cells. *Advanced Science* **2017**, 10.1002/advs.201700031, 1700031-n/a.

[25] Ahn, N.;Son, D.-Y.;Jang, I.-H.;Kang, S. M.;Choi, M.; Park, N.-G. Highly Reproducible Perovskite Solar Cells with Average Efficiency of 18.3% and Best Efficiency of 19.7% Fabricated via Lewis Base Adduct of Lead(II) Iodide. *Journal of the American Chemical Society* **2015**, *137*, 8696-8699.

[26] Jiang, Q.;Zhang, L.;Wang, H.;Yang, X.;Meng, J.;Liu, H.;Yin, Z.;Wu, J.;Zhang, X.; You, J. Enhanced electron extraction using SnO2 for high-efficiency planar-structure HC(NH2)2PbI3-based perovskite solar cells. *Nature Energy* **2016**, *2*, 16177.

[27] Wang, Z.;Lin, Q.;Chmiel, F. P.;Sakai, N.;Herz, L. M.; Snaith, H. J. Efficient ambient-air-stable solar cells with 2D–3D heterostructured butylammonium-caesium-formamidinium lead halide perovskites. *Nature Energy* **2017**, *2*, 17135.

[28] McMeekin, D. P.;Sadoughi, G.;Rehman, W.;Eperon, G. E.;Saliba, M.;Hörantner, M. T.;Haghighirad, A.;Sakai, N.;Korte, L.;Rech, B.;Johnston, M. B.;Herz, L. M.; Snaith, H. J. A mixed-cation lead mixed-halide perovskite absorber for tandem solar cells. *Science* **2016**, *351*, 151-155.

[29] Seo, J.-Y.;Matsui, T.;Luo, J.;Correa-Baena, J.-P.;Giordano, F.;Saliba, M.;Schenk, K.;Ummadisingu, A.;Domanski, K.;Hadadian, M.;Hagfeldt, A.;Zakeeruddin, S. M.;Steiner, U.;Grätzel, M.; Abate, A. Ionic Liquid Control Crystal Growth to Enhance Planar Perovskite Solar Cells Efficiency. *Advanced Energy Materials* **2016**, *6*, 1600767-n/a.

[30] Zhang, F.;Zhao, X.;Yi, C.;Bi, D.;Bi, X.;Wei, P.;Liu, X.;Wang, S.;Li, X.;Zakeeruddin, S. M.; Grätzel, M. Dopant-free star-shaped hole-transport materials for efficient and stable perovskite solar cells. *Dyes and Pigments* **2017**, *136*, 273-277.

[31] Ball, J. M.;Stranks, S. D.;Horantner, M. T.;Huttner, S.;Zhang, W.;Crossland, E. J. W.;Ramirez, I.;Riede, M.;Johnston, M. B.;Friend, R. H.; Snaith, H. J. Optical properties and limiting photocurrent of thin-film perovskite solar cells. *Energy & Environmental Science* **2015**, *8*, 602-609.

[32] Pacchioni, G.; Freund, H. Electron Transfer at Oxide Surfaces. The MgO Paradigm: from Defects to Ultrathin Films. *Chemical Reviews* **2013**, *113*, 4035-4072.

[33] Han, G. S.;Chung, H. S.;Kim, B. J.;Kim, D. H.;Lee, J. W.;Swain, B. S.;Mahmood, K.;Yoo, J. S.;Park, N.-G.;Lee, J. H.; Jung, H. S. Retarding charge recombination in perovskite solar cells using ultrathin MgO-coated TiO2 nanoparticulate films. *Journal of Materials Chemistry A* **2015**, *3*, 9160-9164.

[34] Unger, E. L.;Hoke, E. T.;Bailie, C. D.;Nguyen, W. H.;Bowring, A. R.;Heumuller, T.;Christoforo, M. G.; McGehee, M. D. Hysteresis and transient behavior in current-voltage measurements of hybrid-perovskite absorber solar cells. *Energy & Environmental Science* **2014**, *7*, 3690-3698.

[35] Wetzelaer, G.-J. A. H.;Scheepers, M.;Sempere, A. M.;Momblona, C.;Ávila, J.; Bolink, H. J. Trap-Assisted Non-Radiative Recombination in Organic–Inorganic Perovskite Solar Cells. *Advanced materials* **2015**, *27*, 1837-1841.

[36] Kavan, L.;Tétreault, N.;Moehl, T.; Grätzel, M. Electrochemical Characterization of TiO2 Blocking Layers for Dye-Sensitized Solar Cells. *The Journal of Physical Chemistry C* **2014**, *118*, 16408-16418.

[37] Yin, Z.;Zheng, Q.;Chen, S.-C.;Cai, D.;Zhou, L.; Zhang, J. Bandgap Tunable Zn1-xMgxO Thin Films as Highly Transparent Cathode Buffer Layers for High-Performance Inverted Polymer Solar Cells. *Advanced Energy Materials* **2014**, *4*, 1301404-n/a.

[38] Mazumder, N.;Bharati, A.;Saha, S.;Sen, D.; Chattopadhyay, K. K. Effect of Mg doping on the electrical properties of SnO2 nanoparticles. *Current Applied Physics* **2012**, *12*, 975-982.

[39] Mercado, C. C.;Knorr, F. J.;McHale, J. L.;Usmani, S. M.;Ichimura, A. S.; Saraf, L. V. Location of Hole and Electron Traps on Nanocrystalline Anatase TiO2. *The Journal of Physical Chemistry C* **2012**, *116*, 10796-10804.

[40] Rakshit, S.; Vasudevan, S. Trap-State Dynamics in Visible-Light-Emitting ZnO:MgO Nanocrystals. *The Journal of Physical Chemistry C* **2008**, *112*, 4531-4537.

[41] Barnes, P. R. F.;Anderson, A. Y.;Juozapavicius, M.;Liu, L.;Li, X.;Palomares, E.;Forneli, A.; O'Regan, B. C. Factors controlling charge recombination under dark and light conditions in dye sensitised solar cells. *Physical Chemistry Chemical Physics* **2011**, *13*, 3547-3558.

[42] Lee, M. M.;Teuscher, J.;Miyasaka, T.;Murakami, T. N.; Snaith, H. J. Efficient Hybrid Solar Cells Based on Meso-Superstructured Organometal Halide Perovskites. *Science* **2012**, *338*, 643-647.

[43] Xiong, L.;Qin, M.;Yang, G.;Guo, Y.;Lei, H.;Liu, Q.;Ke, W.;Tao, H.;Qin, P.;Li, S.;Yu, H.; Fang, G. Performance enhancement of high temperature SnO2-based planar perovskite solar cells: electrical characterization and understanding of the mechanism. *Journal of Materials Chemistry A* **2016**, *4*, 8374-8383.

[44] Adachi, D.;Hernández, J. L.; Yamamoto, K. Impact of carrier recombination on fill factor for large area heterojunction crystalline silicon solar cell with 25.1% efficiency. *Applied Physics Letters* **2015**, *107*, 233506.

[45] Bartesaghi, D.;Pérez, I. d. C.;Kniepert, J.;Roland, S.;Turbiez, M.;Neher, D.; Koster, L. J. A. Competition between recombination and extraction of free charges determines the fill factor of organic solar cells. *Nature Communications* **2015**, *6*, 7083.

[46] Kim, H.-S.; Park, N.-G. Parameters Affecting I–V Hysteresis of CH3NH3PbI3 Perovskite Solar Cells: Effects of Perovskite Crystal Size and Mesoporous TiO2 Layer. *The Journal of Physical Chemistry Letters* **2014**, *5*, 2927-2934.

[47] Zaban, A.;Greenshtein, M.; Bisquert, J. Determination of the Electron Lifetime in Nanocrystalline Dye Solar Cells by Open-Circuit Voltage Decay Measurements. *ChemPhysChem* **2003**, *4*, 859-864.

[48] Agresti, A.;Pescetelli, S.;Cinà, L.;Konios, D.;Kakavelakis, G.;Kymakis, E.; Carlo, A. D. Efficiency and Stability Enhancement in Perovskite Solar Cells by Inserting Lithium-Neutralized Graphene Oxide as Electron Transporting Layer. *Advanced Functional Materials* **2016**, *26*, 2686-2694.

[49] Tress, W.;Correa Baena, J. P.;Saliba, M.;Abate, A.; Graetzel, M. Inverted Current–Voltage Hysteresis in Mixed Perovskite Solar Cells: Polarization, Energy Barriers, and Defect Recombination. *Advanced Energy Materials* **2016**, *6*, 1600396-n/a.

[50] Yuan, Y.; Huang, J. Ion Migration in Organometal Trihalide Perovskite and Its Impact on Photovoltaic Efficiency and Stability. *Accounts of Chemical Research* **2016**, *49*, 286-293.

[51] Chen, C.-Y.;Chang, J.-H.;Chiang, K.-M.;Lin, H.-L.;Hsiao, S.-Y.; Lin, H.-W. Perovskite Photovoltaics for Dim-Light Applications. *Advanced Functional Materials* **2015**, *25*, 7064-7070.

[52] Mathews, I.;King, P. J.;Stafford, F.; Frizzell, R. Performance of III–V Solar Cells as Indoor Light Energy Harvesters. *IEEE Journal of Photovoltaics* **2016**, *6*, 230-235.

[53] Freitag, M.;Teuscher, J.;Saygili, Y.;Zhang, X.;Giordano, F.;Liska, P.;Hua, J.;Zakeeruddin, S. M.;Moser, J.-E.;Grätzel, M.; Hagfeldt, A. Dye-sensitized solar cells for efficient power generation under ambient lighting. *Nat Photon* **2017**, *11*, 372-378.

[54] Dagar, J.;Scarselli, M.;De Crescenzi, M.; Brown, T. M. Solar Cells Incorporating Water/Alcohol-Soluble Electron-Extracting DNA Nanolayers. *ACS Energy Letters* **2016**, *1*, 510-515.

- New architectures in $CH_3NH_3PbI_3$ based planar perovskite solar cells incorporating solution processed SnO_2/MgO composite electron transport layers.
- Cells shows highest power outputs ever reported under typical 200-400 lx indoor illumination conditions.
- When measured under white OSRAM LED lamp (200, 400 lx), the maximum power density values were 20.2 μW/cm^2 (estimated PCE = 25.0%) at 200 lx and 41.6 μW/cm^2 (PCE = 26.9%) at 400 lx which correspond to a ~ 20% increment compared to solar cells with a SnO_2 layer only.
- The maximum power conversion efficiency was 19.0% under 1 sun illumination of the best cell with a stabilized value of 18.1%.

- All layers of the cells, except for the two electrodes, are solution processed at low temperatures, thus low cost processing.

- The thin MgO overlayer leads to more uniform films, reduces interfacial carrier recombination, and leads to better stability.

- Furthermore, ambient indoor conditions represent a milder environment compared to stringent outdoor conditions for a technology that is still looking for a commercial outlet also due to stability concerns.

TOC Graphic